Int. J. Electrochem. Sci., 15 **(2020)** 8536 – 8551, doi: 10.20964/2020.09.47

International Journal of ELECTROCHEMICAL SCIENCE
www.electrochemsci.org

Polyaniline Nanofibers Modified Ni Electrodes for Electrochemical Hydrogen Production

Andrea Kellenberger[1], *Daniela Ambros*[1], *Nicoleta Plesu*[2,*]

[1] Politehnica University Timisoara, Faculty of Industrial Chemistry and Environmental Engineering, P-ta Victoriei 2, 300006 Timisoara, Romania
[2] Romanian Academy, Institute of Chemistry, Bd.Mihai Viteazul 24, 300223 Timisoara, Romania
[*]E-mail: plesu_nicole@yahoo.com

Received: 15 May 2020 / *Accepted:* 30 June 2020 / *Published:* 10 August 2020

Polyaniline (PANI) nanofibers have been prepared by potentiodynamic electrodeposition on nickel from aniline in sulfuric acid solution. By varying the scan rate during deposition, polyaniline nanofibers with different diameter and length have been obtained, as shown by scanning electron microscopy. The layer of polyaniline nanofibers deposited on nickel has an open and porous structure at low scan rates and a more compact structure at high scan rates. The modified Ni/PANI electrodes were used for the hydrogen evolution reaction and their electrocatalytic activity was evaluated by linear Tafel polarization and electrochemical impedance spectroscopy in 0.5 M H_2SO_4 solution. It has been shown that the presence of polyaniline nanofibers layer increases the electrocatalytic activity for hydrogen evolution reaction as compared to plain nickel electrode, as indicated by the increase of the apparent exchange current density by two orders of magnitude and the decrease of overpotential for hydrogen evolution reaction.

Keywords: Hydrogen evolution reaction, polyaniline, nanofibers, nickel, water electrolysis

1. INTRODUCTION

Renewable energies remain a promising way to solve the energy and environment crisis. The future perspectives rely on the possibility to use solar cells, wind energy, global thermal energy and bio mass. All of the above mentioned possibilities seems to be more eco-friendly than today energies based on fossil fuels. The friendliest fuel to the environment is hydrogen, which is easy to produce and shows the highest energy density (143 kJ g^{-1}; which is much higher than that of other fuels such as methane) as well as wide applications.

Hydrogen can be obtained by water electrolysis in alkaline or proton exchange membrane (PEM) electrolyzers. Many scientific researchers are motivated to investigate new electrocatalysts for hydrogen evolution reaction (HER), in order to achieve more effective, stable and low-cost electrocatalysts for water splitting in the PEM electrolyzer. These new catalysts should exhibit low overpotentials for the HER at quite high operating current densities (1-2 A cm^{-2}), thus contributing to lowering the production cost of hydrogen. Up to now, platinum remains the best catalyst for HER [1-3] with high exchange current density of 4.5×10^{-4} A cm^{-2} and low Tafel slope (30 mV $decade^{-1}$). The two kinetic parameters that describe charge transfer reaction in HER, the exchange current density i_o and Tafel slope b, are considered suitable criteria in evaluating the electrocatalytic activity of various materials. Besides the intrinsic electrocatalytic effect of the material, an increased active surface area is also beneficial for HER [4-6]. Considering high costs of platinum and limitations for industrial scale use, the investigations were extended to other, more accessible materials with comparable catalytic activity. One of the most commonly investigated metal as a replacement for platinum is nickel and its alloys [7-9], but its use is restricted to alkaline solutions. Recent trends in research include the study of nickel nanoparticles supported on highly active surface area materials such as carbon nanofibers, carbon paper and graphenes as efficient electrocatalysts for HER [10-14]. Other materials with porous structure and highly active surface area used for the development of electrocatalysts for HER are conducting polymers. Polyaniline on platinum [15,16] and polyaniline on glassy carbon substrate [17] have been used for hydrogen evolution reaction in aqueous and respectively non-aqueous media. Results have shown that HER is inhibited due to the presence of PANI on platinum, because HER is taking place in fact on the underlying platinum substrate and PANI acts as a barrier towards electrolyte solution [15]. More often, conducting polymers are used as three-dimensional (3D) matrices for electrodeposition of active metals such as nickel [18,19] or for the preparation of nickel/Pani composites [20,21]. Conductive polyaniline nanowires were used to construct a 3D hybrid electrocatalyst with MoS_2, resulting in a 3D hydrogen evolution zone, thus increasing the surface area and the number of active sites as compared to a flat, two dimensional conducting substrate [22]. The electrocatalytic activity of electrodes obtain by the codeposition of polyaniline particles with nickel, has been investigated and revealed that a higher PANI particle content in the composite enhances catalytic activity for the HER, as reflected by a decrease of overpotential and charge transfer resistance values and the increase of exchange current density [20]. Another study investigated the electrocatalytic activity of electrocatalysts produced by electrodeposition of Ni and NiMo layers on/in a preformed PANI. Two effects have been found to contribute to an enhanced electrocatalytic activity for HER: the increase in surface roughness achieved by using PANI matrix and the increase of intrinsic activity of the material achieved by alloying Ni with Mo [19]. Until now, the studies have shown that the structure of the conductive polymer layer and the nature of conductive polymer/electrode surface /electrolyte interface strongly depends on the morphology of the prepared conductive polymer layers and the type of polymer [23-26].

In the present work, we used PANI as a conductive polymer layer electrodeposited on Ni substrate and determined the electrocatalytic activity of Ni/PANI layers for HER. The effect of polyaniline morphology upon the electrocatalytic activity of Ni/PANI electrodes was investigated using as a parameter the scan rate applied for the potentiodynamic deposition of the polymer films. It has been shown that the highest electrocatalytic activity is obtained for the lowest deposition scan rate, which corresponds to the formation of a network of long nanofibers with an increased surface area. We demonstrate that PANI layer can act not only as a matrix but also as an active material for HER. The increased electrocatalytic activity of Ni/PANI electrodes has been explained based on the existence of abundant protonated amine sites, which can be regarded as fixed proton sources, able to increase the concentration of protons in the close vicinity of the metal/electrolyte interface and thus enhance the rate of hydrogen evolution reaction.

2. EXPERIMENTAL

2.1. Materials

Before use aniline (puriss., p.a., ≥ 99.5% GC from Fluka) was purified by distillation under reduced pressure and stored in a dark recipient at low temperature. Electrolyte solutions were prepared using sulfuric acid (95-97% p.a. from Merck). Electrodes were manufactured from a nickel plate (99.2% Ni) by cutting disk-shaped samples with 15 mm diameter. Before use, the surface of the nickel disk electrodes was prepared by polishing with SiC paper of different grades (from 400 to 2400 µm) followed by mirror polishing with diamond sprays of different grain size (6 and 3 µm). Between the polishing steps, the electrode was thoroughly rinsed and ultrasonicated in distilled water. After preparation, the electrode was immediately immersed in the sulfuric acid solution.

2.2. Synthesis of Ni/PANI electrodes

An Autolab PGSTAT 302N potentiostat was used to perform the electrochemical measurements. The electrochemical cell was a conventional three-electrode one-compartment glass cell, containing a nickel disk working electrode ($S = 0.64$ cm^2), graphite rods counter electrodes and a silver/silver chloride (Ag/AgCl) reference electrode. The electrochemical deposition of polyaniline was performed by cyclic voltammetry from an aqueous solution of 0.1 mol L^{-1} aniline in 0.5 mol L^{-1} H_2SO_4. The polymerization was initiated by sweeping the potential from –0.15 V to 1.25 V during the first three cycles. Afterwards, the reversal potential was decreased to 0.85 V and the potential was cycled between –0.15 V and 0.85 V for the next cycles. Polymer films with different thickness and morphology were obtained by varying the scan rate during deposition from 10 to 25 and 50 mV s^{-1}, similarly to those described in our previous work [24]. The corresponding samples are denoted as Ni/PANI/10, Ni/PANI/25 and Ni/PANI/50.

2.3. Characterization of the Ni/PANI electrodes

Field emission scanning electron microscopy (FE-SEM) was used to characterize the structure and morphology of Ni/PANI electrodes. FE-SEM images were taken with a QUANTA FEG 250 scanning electron microscope. The redox properties of electrochemically prepared Ni/PANI layers were investigated by cyclic voltammetry in 0.5 mol L^{-1} H_2SO_4 solution.

Linear voltammetry and electrochemical impedance spectroscopy (EIS) were used to characterize the electrocatalytic effect of Ni/PANI electrodes on the hydrogen evolution reaction. Steady-state polarization curves were recorded in 0.5 mol L^{-1} H_2SO_4 solution with a scan rate of 1 mV s^{-1}. EIS measurements were carried out using the FRA module of Autolab 302 N. Data were collected in the frequency range from 100 kHz to 100 mHz with an AC voltage amplitude of 10 mV. Each spectrum consisted of 60 points, with a logarithmic distribution of 10 points per decade. A complex non-linear least squares (CNLS) Levenberg–Marquardt procedure was used to fit the experimental electrochemical impedance data to the equivalent electric circuit, using the ZView 3.0 software (Scribner Associates, Inc.).

3. RESULTS AND DISCUSSION

3.1. Synthesis and characterization of Ni/PANI electrodes

Cyclic voltammograms obtained during electrochemical oxidation of aniline on nickel are given in Figure 1. The first anodic scan corresponds to the passivation of the nickel surface as indicated by an irreversible oxidation peak attributed to the formation of nickel oxide. The absence of this peak in the further scans indicates that a passive oxide film covers the electrode, allowing the electrooxidation of aniline monomer and further growth of PANI film.

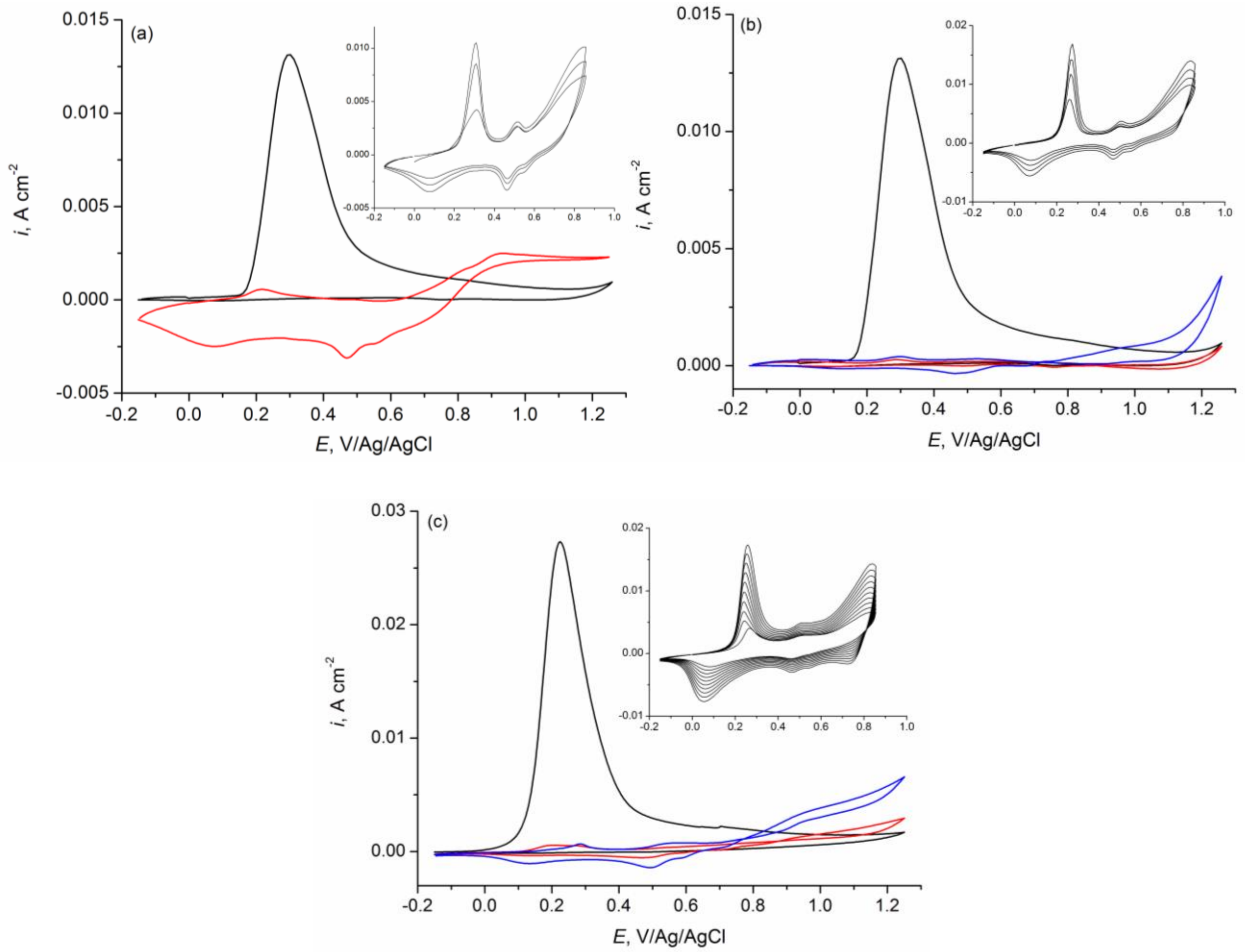

Figure 1. Cyclic voltammograms during the initiation step of PANI electropolymerization from 0.1 mol L^{-1} aniline in 0.5 mol L^{-1} H_2SO_4 solution at different scan rates: 10 (a); 25 (b) and 50 mV s^{-1} (c). Inset: corresponding voltammograms of the growth step.

The CVs obtained during the growth of PANI films, given as inset in Figure 1, reveal the presence of two main pairs of redox peaks whose intensity increases continuously during potential cycling. This is a typical behavior of electrochemically synthesized PANI, as reported in the literature [27-29], and the two pairs of peaks have been identified as the redox transitions of PANI from the fully reduced oxidation state leucoemeraldine to the half-oxidized state emeraldine and respectively from emeraldine to the fully oxidized state pernigraniline [30-32]. The CVs in Figure 1 also show the existence of an intermediate pair of redox peaks, which has been ascribed to secondary degradation reactions of the PANI chain [30,33,34]. The peak potential of the first redox transition is scan rate dependent and it shifts slightly to more negative potentials as the scan rate increases. The scan rate also affects the intensity of the degradation peaks, their intensity becomes more pronounced at lower scan rates.

The redox activity of Ni/PANI electrodes obtained at different scan rates was investigated by cyclic voltammetry in monomer free sulfuric acid solution. A classical behavior for conducting polyaniline is observed, as seen in Figure 2. The first anodic peak corresponding to the redox transition from leucoemeraldine to emeraldine is roughly centered at 0.38 V for Ni/PANI/10, at 0.34 V for Ni/PANI/25 and at 0.26 V for Ni/PANI/50. Its position shifts to higher potentials as the scan rate is lowered and the thickness of the polymer film increases.

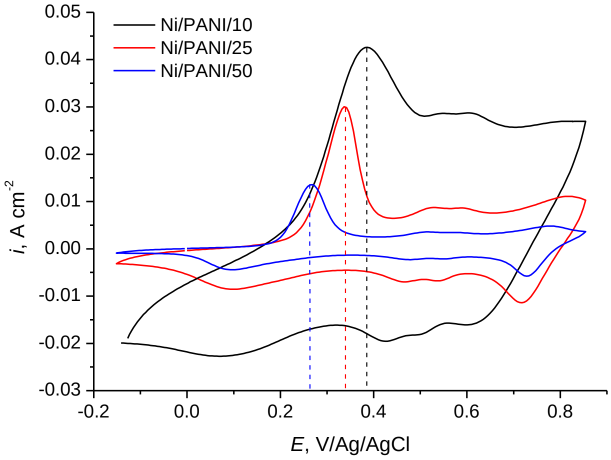

Figure 2. Cyclic voltammograms of Ni/PANI layers obtained by electropolymerization at different scan rates, in monomer free 0.5 mol L^{-1} H_2SO_4 solution. Scan rate 50 mV s^{-1}.

In a previous work we have shown that the morphology of PANI electrochemically deposited on nickel is controlled by the scan rate applied during the potentiodynamic deposition [24]. Figure 3 gives the FE-SEM images of Ni/PANI electrodes obtained using different scan rates.

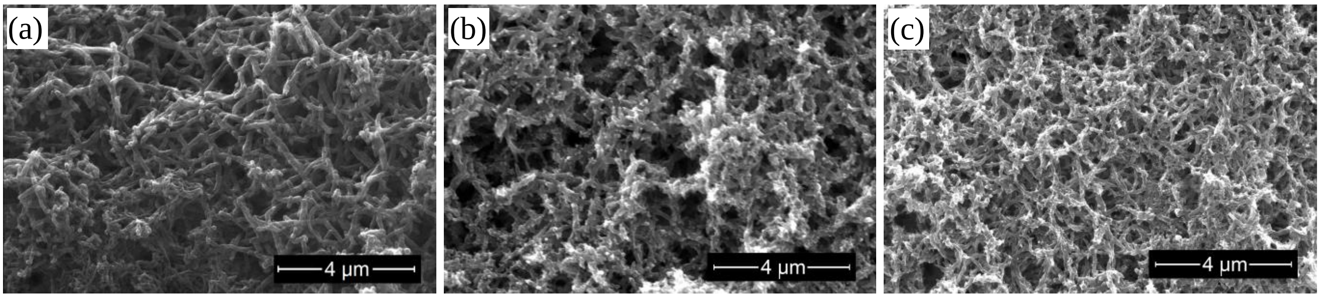

Figure 3. FE-SEM images of Ni/PANI/10 (a), Ni/PANI/25 (b) and Ni/PANI/50 (c) electrodes.

It can be observed that at low scan rates the nanofibrilar morphology predominates whereas at higher scan rates granular PANI is also obtained. The average diameter and length of the nanofibers are controlled by the deposition scan rate. At low scan rates thicker and longer nanofibers are obtained and at high scan rates thinner and shorter nanofibers are formed as a result of different nucleation mechanism. In addition, the network of PANI nanofibers shows a more open and porous structure at low scan rates as compared to a more compact structure at high scan rates.

3.2. HER on Ni/PANI electrodes

Steady-state polarization curves, given in Figure 4a, were recorded potentiostatically in 0.5 M H_2SO_4 solution to evaluate the electrocatalytic activity of Ni/PANI electrodes towards HER, and the corresponding Tafel plots were obtained, as seen in Figure 4b.

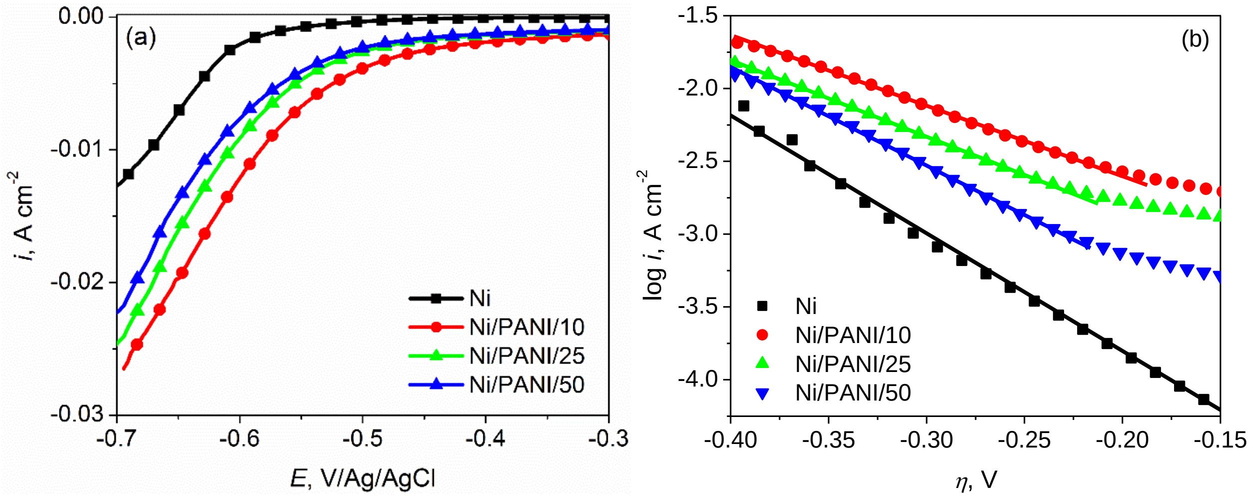

Figure 4. Steady-state polarization curves (a) and Tafel plots (b) for HER on Ni and Ni/PANI electrodes in 0.5 M H_2SO_4 solution at 20°C.

It can be observed that all Ni/PANI electrodes have some catalytic effect compared to a plain Ni electrode, by decreasing the potential needed for hydrogen evolution reaction at a constant current density. The most significant effect, of about 100 mV decrease of the overpotential at a current density of 100 A m^{-2} has been observed for Ni/PANI/10 electrode.

Table 1. Kinetic parameters for HER on Ni and Ni/PANI electrodes in 0.5 M H_2SO_4 solution at 20°C.

Electrode	b (mV dec^{-1})	1-α	i_o (A cm^{-2})	i (mA cm^{-2}) at -150 mV	η (mV) at 1 mA cm^{-2}
Ni	-118	0.50	2.9×10^{-6}	-0.06	-300
Ni/PANI/50	-148	0.31	6.5×10^{-5}	-1.18	-230
Ni/PANI/25	-190	0.30	1.4×10^{-4}	-1.38	-173
Ni/PANI/10	-207	0.29	3.1×10^{-4}	-2.00	-117

According to the Tafel plots from Figure 4b, the highest difference in the electrocatalytic effect is observed at low overpotentials and it becomes less important at higher overpotentials. More conclusive information about the electrocatalytic effect is given by the kinetic parameters (Tafel slope b, exchange current density i_o and charge transfer coefficient 1-α) derived from the Tafel plots. The values of kinetic parameters are given in Table 1.

The apparent exchange current density i_o, provides information about the electrocatalytic activity of the electrode and according to the data from Table 1, it is observed that the exchange current density value increases in the order: Ni < Ni/PANI/50 < Ni/PANI/25 < Ni/PANI/10. Compared with the nickel electrode, all of the Ni/PANI electrodes showed higher exchange current densities, indicating that the presence of PANI on the surface of the electrodes accelerates HER. The 100-fold increase of exchange current density value for Ni/PANI/10 indicates that HER take place with the highest rate on the Ni/PANI electrode obtained at the lowest scan rate. This suggests that not only the presence of PANI but also its morphology has an effect on the electrocatalytic activity.

Table 2. Comparison of HER performance of PANI based electrocatalysts in acid media.

Catalyst / Preparation	b (mV dec^{-1})	i_o (μA cm^{-2})	η (mV) at 1 mA cm^{-2}	i (mA cm^{-2}) at -150 mV	Ref.
Ni/PANI-20/5 / Potentiostatic electrodeposition of PANI on GC followed by electrodeposition of Ni	-133	47	-175	-0.647	[18]
Ni/PANI / Potentiostatic electrodeposition of PANI on GC followed by electrodeposition of Ni	-156	27	-259	-0.215	[19]
Ni-PAni 175 / Codeposition of Ni with 175 g L^{-1} PAni particles on GC	-131	239	-82	-3.25	[20]
Ni/PANI/10 / Potentiodynamic electrodeposition of PANI on Ni, scan rate 10 mV s^{-1}	-207	310	-117	-2.0	this work

According to the Butler-Volmer equation, a high Tafel slope and a low charge transfer coefficient 1–α are disadvantageous for HER kinetics, because only a smaller fraction of the interfacial potential is used in activating the reactants to the top of the free energy barrier. In terms of reaction coordinates, a lower value of 1–α means that the reaction plane is farther away from the metal surface. This is the case of polyaniline layers of different thicknesses present on the surface of nickel electrode, with the lowest value of charge transfer coefficient obtained for the thickest layer Ni/PANI/10. However, the decrease of 1–α is compensated by the important increases of the exchange current density i_o and as a result, the overall effect of polyaniline layers on nickel is to accelerate HER at low overpotentials. A similar electrocatalytic effect on HER in acid solutions has been observed in the presence of aromatic amines [35-38]. These electrocatalysts in the solution, also called proton carriers, have the ability to coordinate protons by the lone pair of electrons of the nitrogen atom and thus to increase the proton concentration in the electric double layer at the metal-solution interface by transporting protons from the solution to the interface. It is obvious that polyaniline, due to its numerous protonated sites may act in a similar way, as a fixed proton source at the metal / electrolyte interface.

The electrocatalytic activity of electrocatalysts for HER under operating conditions can also be evaluated by comparing current density values at the same overpotential or the overpotential necessary to sustain a certain current density. The results for an overpotential of −150 mV, which is usually expected during hydrogen production, are given in Table 1. The highest current density is obtained for Ni/PANI/10, which offers an about 30 time higher overall electrocatalytic activity than the Ni electrode. These results have been compared in Table 2 with information reported on composite coatings obtained by electrodeposition of nickel in the presence polyaniline particles [20] or directly inside a previously formed three-dimensional polyaniline matrix [18,19].

Electrochemical impedance spectroscopy was used further to characterize HER on Ni/PANI modified electrodes as compared to a simple Ni electrode. Impedance spectra were recorded at room temperature for different values of the electrode overpotential as shown in Figure 5.

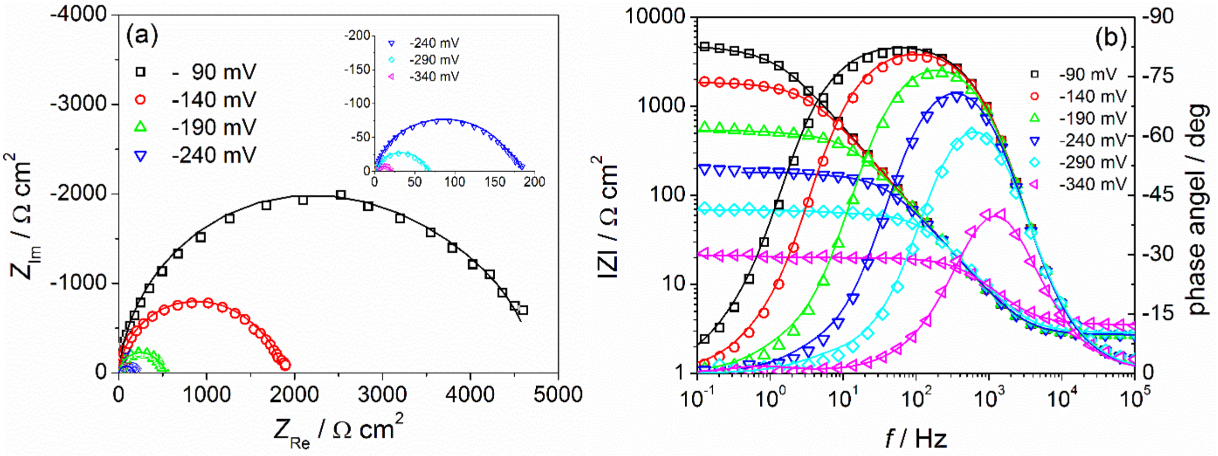

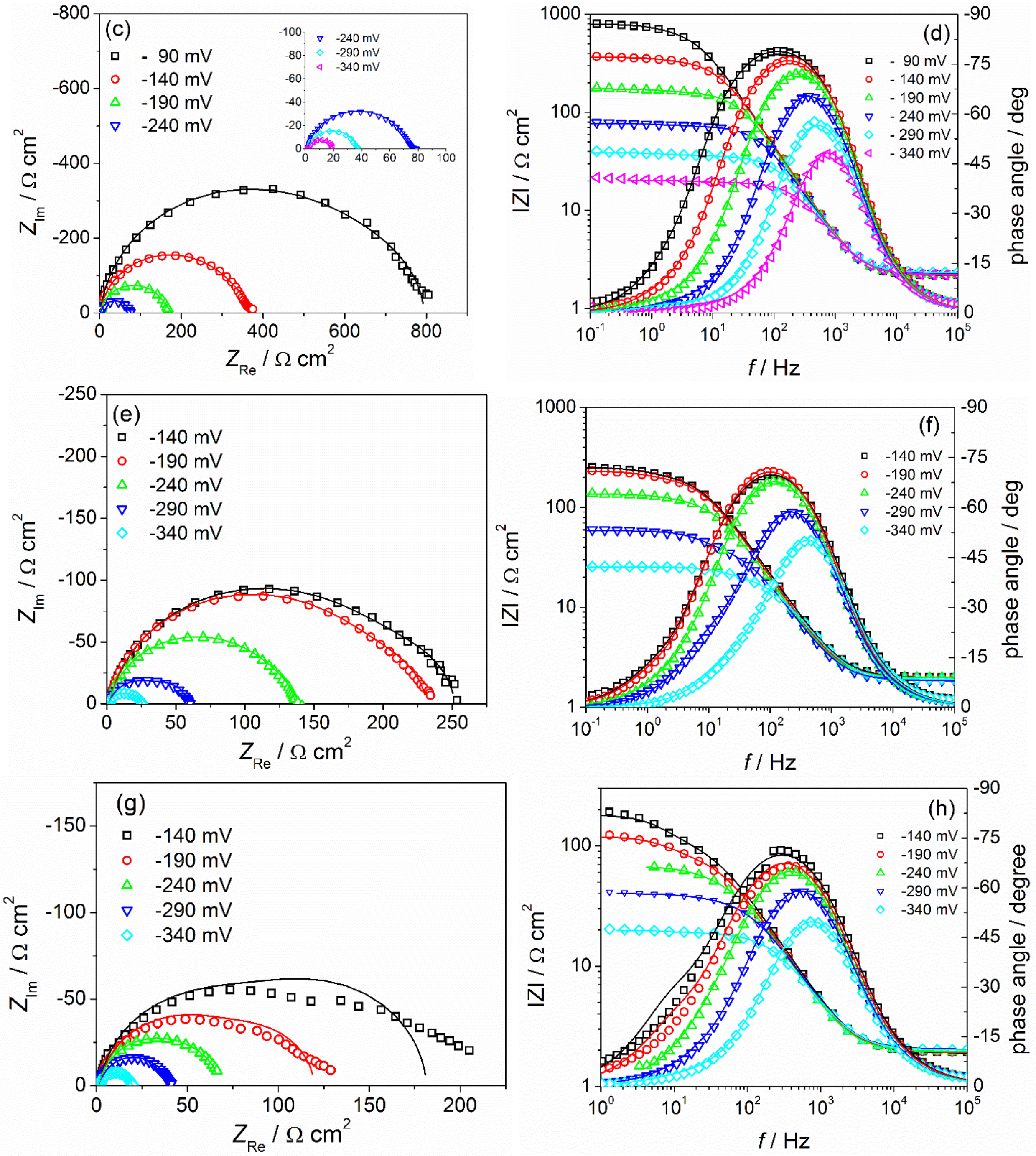

Figure 5. Experimental (symbols) and simulated (solid lines) complex plane and Bode plots for hydrogen evolution reaction in 0.5 M H_2SO_4 solution on Ni (a, b); Ni/PANI/50 (c, d); Ni/PANI/25 (e, f) and Ni/PANI/10 (g, h) electrode at different overpotentials.

The complex plane plots for HER on Ni show the presence of only one depressed semicircle whose diameter decreases with increasing overpotential. This reflects a decrease of the charge transfer resistance of HER. In case of Ni/PANI electrodes, the semicircles are not perfectly symmetrical, but show some deviations at low frequencies, which indicate a more complex response than a single time constant behavior. This feature is more evident at low overpotentials and tends to disappear at high overpotentials, where EIS spectra tend to become similar on all tested electrodes, which is also in accordance with observations from steady-state polarization curves. To model this behavior, two different electrical equivalent circuits (EEC) have been used, as shown in Figure 6. The first circuit is a one-time constant model and contains the solution resistance (R_S) in series with two parallel components: a constant phase element (CPE-1) and a resistance R_1. The second circuit is a two-time constants model and contains an additional time constant expressed by a constant phase element (CPE-2) and a resistance R_2.

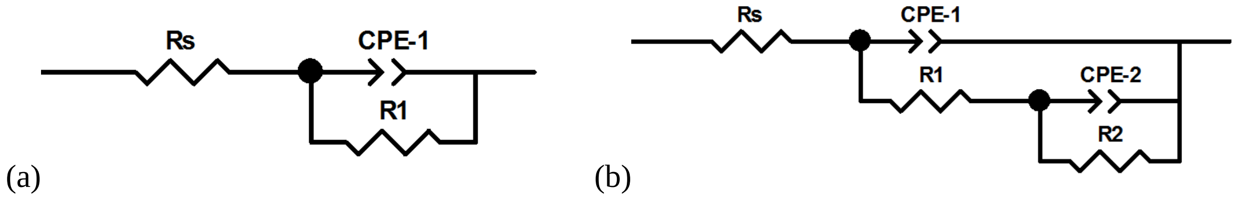

(a) (b)

Figure 6. Electric equivalent circuit for hydrogen evolution reaction in 0.5 M H_2SO_4 solution on Ni (a) and Ni/PANI (b) electrodes.

In both circuits, the ideal capacitance was replaced by a constant phase element (CPE) to account for the non-ideality of the surface, with the impedance of CPE given by:

$$Z_{CPE} = \frac{1}{T(j\omega)^n} \qquad (3)$$

where *T* is a parameter related to the double layer capacitance according to relation (4) and *n* is parameter between 0 and 1 describing the constant phase angle of the CPE, which is *n**90°:

$$T_i = C_{dl,i}^n (R_s^{-1} + R_i^{-1})^{1-n} \qquad (4)$$

The model presented in Figure 6a fitted very well the impedance results on plain Ni electrode, with standard errors below 5% for all the parameters. The values of the EIS parameters are given in Table 3 together with the goodness of fit expressed by the χ^2 value, the calculated double layer capacitance and time constant values.

Table 3. Fitting results of impedance spectra for HER on Ni in 0.5 M H_2SO_4 solution.

η (mV)	R_S (Ω)	CPE-1 (F cm^{-2} s^{n-1})	n_1	R_1 (Ω cm^2)	C_1 (μF cm^{-2})	τ_1 (s)	χ^2
-90	2.7	3.44×10^{-5}	0.94	4520	39	1.7×10^{-1}	1.8×10^{-3}
-140	2.7	3.45×10^{-5}	0.94	1805	39	7.0×10^{-2}	1.2×10^{-3}
-190	2.7	3.62×10^{-5}	0.94	523	41	2.2×10^{-2}	3.8×10^{-3}
-240	2.7	3.52×10^{-5}	0.94	172	40	6.8×10^{-3}	1.2×10^{-3}
-290	2.9	3.55×10^{-5}	0.93	63	41	2.6×10^{-3}	4.1×10^{-3}
-340	3.5	3.82×10^{-5}	0.92	17	45	7.5×10^{-4}	7.6×10^{-3}

The values of resistance R_1 show an important decrease with increasing overpotential. Meanwhile, the capacitance values remain constant, with a very small standard deviation (40.8 ± 2.0 µF cm^{-2}). As a result, the corresponding time constant decreases with overpotential. This is a typical response of HER charge transfer resistance expressed by R_1 and of double layer capacitance expressed by CPE-1. Accordingly, HER charge transfer kinetics is described by the first time constant. Literature data indicate that the double layer capacitance of a smooth metal electrode is 20 µF cm^{-2} [39], therefore the roughness factor of the plain Ni electrode can be estimated at about 2.

EIS data on Ni/PANI electrodes were very well fitted using the two-time constants model presented in Figure 6b. The values of the EIS parameters obtained after fitting are given in Table 4 for Ni/PANI/50, Table 5 for Ni/PANI/25 and Table 6 for Ni/PANI/10, together with the goodness of fit expressed by the χ^2 value, the calculated double layer capacitance and time constant values. Only standard errors of CPE-2 and R_2 parameters are indicated, as all the other parameters showed errors less than 10%. At high overpotentials, the standard error for fitting of parameters CPE-2 and R_2 tends to increase, which is consistent with the disappearance of the second semicircle and the EIS spectra could be modelled to the EEC shown in Figure 6a.

In case of Ni/PANI electrodes, the values of resistance R_1 progressively decrease and the capacitance values are relatively constant with increasing overpotential. The double layer capacitance shows insignificant variation, indicating that the surface blockage by produced molecular hydrogen is minor. The capacitance values are respectively 58.6 ± 5.4 µF cm^{-2} (Ni/PANI/50) 172.1 ±13.3 µF cm^{-2} (Ni/PANI/25) and 65.0 ± 6.7 µF cm^{-2} (Ni/PANI/10). Consequently, the first time constant decreases with overpotential and it can be ascribed to HER charge transfer kinetics. Regarding the second time constant, it is obviously also overpotential dependent but the capacitance values C_2 increase and the resistance values R_2 decrease at higher overpotentials. A change of capacitance values with overpotential indicate a different response than that of double layer, namely that of adsorbed hydrogen on the electrode surface. Accordingly, the second time constant is related to hydrogen adsorption process and the corresponding parameters C_2 and R_2 are ascribed to hydrogen adsorption pseudocapacitance and respectively resistance. The first time constant τ_1 related to charge transfer has smaller values that the second time constant τ_2 related to hydrogen adsorption. Therefore, for the Ni/PANI electrodes, the high frequency semicircle corresponds to charge transfer and the low frequency semicircle to hydrogen adsorption.

Kinetic parameters may be also determined from EIS data. At low overpotentials, the linearization of the Butler Volmer equation allows to estimate the charge transfer resistance given by equation (5).

$$R_{ct} = \frac{RT}{nFi_o} \qquad (5)$$

The values of exchange current density i_o have been determined based on equation (5) using the charge transfer resistance values determined by EIS at the lowest overpotential measured and compared to i_o values obtained by the linear Tafel polarization method, as indicated in Table 7.

Table 4. Fitting results of the impedance spectra for HER on Ni/PANI/50 in 0.5 M H_2SO_4 solution.

η (mV)	R_S (Ω)	CPE-1 (F s^{n-1} cm^{-2})	n_1	R_1 (Ω cm^2)	C_1 (μF cm^{-2})	τ_1 (s)	CPE-2 (F s^{n-1} cm^{-2})	n_2	R_2 (Ω cm^2)	C_2 (μF cm^{-2})	τ_2 (s)	χ^2
-90	2.2	4.90×10^{-5}	0.95	689	54	3.7×10^{-2}	1.01×10^{-3} (13%)	0.85	96 (5%)	1333	12.8×10^{-2}	1.7×10^{-4}
-140	2.2	4.80×10^{-5}	0.95	331	53	1.7×10^{-2}	2.34×10^{-3} (15%)	0.87	29 (6%)	2951	8.6×10^{-2}	1.7×10^{-4}
-190	2.2	4.98×10^{-5}	0.95	158	55	0.9×10^{-2}	5.98×10^{-3} (20%)	0.88	10 (8%)	7300	7.4×10^{-2}	2.7×10^{-4}
-240	2.3	5.30×10^{-5}	0.95	70	59	0.4×10^{-2}	8.04×10^{-3} (20%)	1.00	2 (17%)	8043	1.5×10^{-2}	7.6×10^{-4}
-290	2.3	5.90×10^{-5}	0.94	34	66	0.2×10^{-2}	-	-	-	-	-	3.6×10^{-4}
-340	2.2	5.98×10^{-5}	0.94	17	66	0.1×10^{-2}	-	-	-	-	-	3.7×10^{-4}

Table 5. Fitting results of the impedance spectra for HER on Ni/PANI/25 in 0.5 M H_2SO_4 solution.

η (mV)	R_S (Ω)	CPE-1 (F s^{n-1} cm^{-2})	n_1	R_1 (Ω cm^2)	C_1 (μF cm^{-2})	τ_1 (s)	CPE-2 (F s^{n-1} cm^{-2})	n_2	R_2 (Ω cm^2)	C_2 (μF cm^{-2})	τ_2 (s)	χ^2
-90	2.0	1.47×10^{-4}	0.88	221	181	4.0×10^{-2}	6.49×10^{-3} (2%)	0.62	210 (7%)	2510	52.7×10^{-2}	1.3×10^{-4}
-140	2.0	1.46×10^{-4}	0.89	217	176	3.8×10^{-2}	5.84×10^{-3} (7%)	0.83	36 (6%)	4128	14.8×10^{-2}	1.5×10^{-4}
-190	2.0	1.44×10^{-4}	0.91	203	169	3.4×10^{-2}	6.57×10^{-3} (8%)	0.91	27 (7%)	5463	14.8×10^{-2}	1.9×10^{-4}
-240	2.0	1.56×10^{-4}	0.91	125	183	2.3×10^{-2}	9.38×10^{-3} (18%)	0.97	9 (13%)	8981	7.8×10^{-2}	2.8×10^{-4}
-290	1.9	1.57×10^{-4}	0.91	38	182	0.7×10^{-2}	1.88×10^{-3} (6%)	0.79	20 (4%)	1065	2.1×10^{-2}	3.4×10^{-4}
-340	1.9	1.27×10^{-4}	0.92	19	145	0.3×10^{-2}	2.73×10^{-3} (10%)	0.85	5 (7%)	1935	1.0×10^{-2}	4.7×10^{-4}

Table 6. Fitting results of the impedance spectra for HER on Ni/PANI/10 in 0.5 M H_2SO_4 solution.

η (mV)	R_S (Ω)	CPE-1 (F s^{n-1} cm^{-2})	n_1	R_1 (Ω cm^2)	C_1 (μF cm^{-2})	τ_1 (s)	CPE-2 (F s^{n-1} cm^{-2})	n_2	R_2 (Ω cm^2)	C_2 (μF cm^{-2})	τ_2 (s)	χ^2
-90	2.0	6.90×10^{-5}	0.93	45	77	3.5×10^{-3}	4.78×10^{-3} (3%)	0.69	21 (2%)	1813	3.9×10^{-2}	9.6×10^{-5}
-140	1.9	5.10×10^{-5}	0.95	94	55	5.2×10^{-3}	5.97×10^{-4} (21%)	0.70	104 (16%)	397	4.1×10^{-2}	4.8×10^{-3}
-190	1.9	5.77×10^{-5}	0.94	75	64	4.8×10^{-3}	1.06×10^{-3} (24%)	0.70	48 (19%)	726	3.5×10^{-2}	2.7×10^{-3}
-240	1.9	5.90×10^{-5}	0.95	56	64	3.6×10^{-3}	1.18×10^{-3} (25%)	0.84	10 (17%)	936	0.9×10^{-2}	1.9×10^{-4}
-290	2.0	5.77×10^{-5}	0.94	34	63	2.2×10^{-3}	8.75×10^{-3} (35%)	0.61	5 (33%)	6274	3.0×10^{-2}	4.2×10^{-4}
-340	2.0	6.28×10^{-5}	0.94	17	69	1.2×10^{-3}	-	-	-	-	-	2.0×10^{-4}

Tafel plots similar to those obtained by dc polarization can also be obtained from EIS measurements. Considering that the overall resistance to HER is represented by the sum of charge transfer resistance R_1 and hydrogen adsorption resistance R_2, and that the current for HER is inversely proportional to the resistance, the semi-logarithmic plot of log $1/(R_1 + R_2)$ versus applied overpotential should give similar representations to that of Tafel plots. The slope's value of this Tafel-like plots (here not shown) are also listed in Table 7. Both linear polarization method and EIS gave very similar values of the kinetic parameters exchange current density i_o and Tafel slope b.

Table 7. Exchange current density and Tafel slope for HER on Ni and Ni/PANI electrodes in 0.5 M H_2SO_4 solution, as determined by linear polarization and electrochemical impedance spectroscopy.

Electrode	i_o (A cm^{-2})		b (mV dec^{-1})	
	Tafel	EIS	Tafel	EIS
Ni	2.9×10^{-6}	5.7×10^{-6}	-118	-103
Ni/PANI/50	6.5×10^{-5}	3.7×10^{-5}	-151	-149
Ni/PANI/25	1.4×10^{-4}	1.2×10^{-4}	-190	-189
Ni/PANI/10	3.1×10^{-4}	5.7×10^{-4}	-207	-193

Figure 7 shows a comparison of complex plane impedance plots for the three Ni/PANI electrodes obtained at different scan rates and for a plain Ni electrode for HER at an overpotential of -90 mV. Their relative electrocatalytic activity was calculated based on the charge transfer resistance values, normalized to the value of plain Ni electrode.

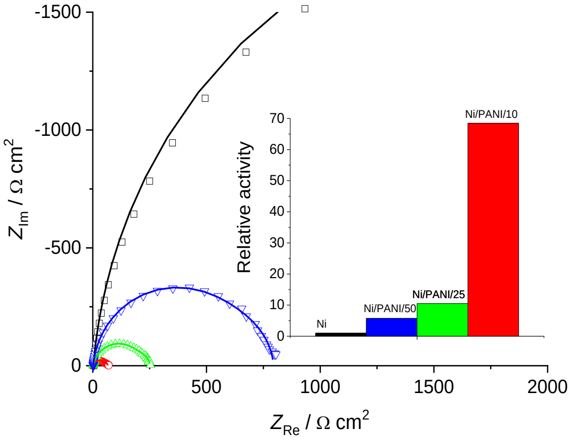

Figure 7. Comparison of complex plane impedance plots for HER on Ni/PANI and Ni electrodes in 0.5 M H_2SO_4 solution and their relative electrocatalytic activity calculated at -90 mV overpotential (inset).

The value of charge transfer resistance decreases in the order: plain Ni > Ni/PANI/50 > Ni/PANI/25 > Ni/PANI/10, similar to the trend of increasing relative electrocatalytic activity. The highest electrocatalytic activity is obtained for Ni/PANI/10, which is about 70 times more active for HER than the plain Ni electrode at the lowest overpotential measured.

The double layer capacitance is directly related to the surface roughness, so to the active surface area involved in the hydrogen evolution reaction. The capacitance of PANI/Ni/10 film is larger than that of PANI/Ni/50 film, as expected due to the increase of the film thickness and quantity of deposited PANI. However, an unusual high capacitance is found for Ni/PANI/25, similarly to our previous results [24]. Despite the higher capacitance and surface roughness of Ni/PANI/25, the best results for HER were obtained on Ni/PANI/10. This means that lower electrocatalytic activity obtained for Ni/PANI/25 may be related to a reduced access of the solution through the pores. In the release of hydrogen, the porous structure depends on the existence of connecting pores (the pores could be more or less regular in their geometry) that brings significant variation in the relaxation time constants. In our situation, both time constants, τ_1 related to charge transfer and τ_2 related to hydrogen adsorption, have higher values for Ni/PANI/25. This indicates a slower charge transfer and a reduced access of electrolyte through the pores (a longer access path), as observed by other authors [40]. The results pointed out to a charge transport within the PANI film complicated by the contacts between agglomerates. The contact between agglomerates decrease with the increase of scan rates and because of polymeric material morphology changes. The results obtained for HER on Ni/PANI/10 reveal a porosity and morphology of the film able to provide superior contact between the substrate and the electrolyte solution. For PANI films obtained at intermediate scan rates (Ni/PANI/50 and Ni/PANI/25) the presence of granular inclusions in the nanofibrilar morphology reduces even more the contacts between PANI chains and as a result, the films present higher values of the charge transfer resistance. Mo et al. [41] made similar observation on polypyrrole (PPy) graphite–paraffin, and found out higher current densities for HER on electrodes modified with fibrillar PPy than on electrodes modified with cauliflower PPy.

4. CONCLUSIONS

Modified Ni/PANI electrodes obtained by electrodeposition of polyaniline at different scan rates on a nickel substrate were tested as cathode materials for hydrogen evolution reaction. SEM images show a transition from nanofiber morphology at low electrodeposition scan rates to a mixed nanofibrilar – granular morphology at higher electrodeposition scan rates. The effect of different PANI morphologies on HER kinetics was investigated by Tafel polarization and electrochemical impedance spectroscopy in in 0.5 M H_2SO_4 solution, as compared to an uncoated, plain Ni electrode. Linear polarization data indicate that all PANI films show an electrocatalytic effect on HER, which is more pronounced at low overpotentials and less important at high overpotentials. Kinetic parameters for HER have been determined and revealed a 100-fold increase of the apparent exchange current density for Ni/PANI/10 as compared to plain Ni electrode. HER takes place on the underlying nickel substrate and the polyaniline nanofibers with numerous protonated amine sites act as a proton source at the metal / polymer / electrolyte interface, thus increasing the protons concentration at the interface and enhancing the HER rate at low overpotentials. At high overpotentials, this effect is less important and the electrocatalytic activity of all PANI films tends to equalize. Electrochemical impedance spectroscopy allowed identifying two time constants for Ni/PANI electrodes, the first one related to HER charge transfer kinetics and the second one to hydrogen adsorption. The charge transfer resistance decreases in the order: plain Ni > Ni/PANI/50 > Ni/PANI/25 > Ni/PANI/10, similar to the trend of increasing apparent exchange current density and relative electrocatalytic activity. The improvement of electrocatalytic effect is also related to an increased surface area of PANI nanofibers. The surface area is linked with the morphology of polymer, which in turn is scan rate dependent. The best electrocatalytic activity was demonstrated by Ni/PANI/10, obtained at low electrodeposition scan rate. Ni/PANI/10 reveals a porosity and morphology of the film able to provide superior contact between the substrate and the electrolyte solution.

References

1. S. Trasatti, *J. Electroanal. Chem. Interf. Electrochem.*, 39 (1972) 163.
2. M. H. Miles and M. A. Thomason, *J. Electrochem. Soc.*, 123 (1976) 1459.
3. A. Eftekhari, *Int. J. Hydrogen Energy*, 42 (2017) 11053.
4. L. Jun and Z. Gengfeng, *Adv. Sci.*, 4 (2017) 1600380
5. S. J. Gutić, A.S. Dobrota, E. Fako, N.V. Skorodumova, N. López and I.A. Pašti, *Catalysts*, 10 (2020) 290.
6. M. Zeng and Y. Li, *J. Mater. Chem*. A, 3 (2015) 14942.
7. P.-C. Chen, Y-M. Chang, P.-W. Wu and Y.-F.Chiu, *Int. J. Hydrogen Energy*, 34 (2009) 6596.
8. X. H. Zhao, M. Fuji, T. Shirai, H. Wanatabe, M. Takahashi and Y. Zuo, *J. Mater. Sci.,* 46 (2011) 4630.
9. C. Adán, F. J. Pérez-Alonso, S. Rojas, M. A. Peña and J.L.G. Fierro, *Int. J. Hydrogen Energy*, 37 (2012) 14984.
10. Q. Ding, M. Liu, Y.-E. Miao, Y. Huang and T. Liu, *Electrochim. Acta,* 159 (2015) 1.
11. J. Li, Y. Zhao, A. Wu and Y. Wang, *Int. J. Electrochem. Sci.*, 14 (2019) 7582.
12. N.K. Mahale and S.T. Ingle, *Energy,* 119 (2017) 872.
13. Wang, Y. Li, M. Xi, Z. Li, Z. Chen, Z. Ma, X. Qin and G. Shao, *J. Power Sources,* 347 (2017) 220.
14. S. J. Gutić, M. Šabanović, D. Metarapi, I. A. Pašti, F. Korać and S. V. Mentus, *Int. J. Electrochem. Sci.,* 14 (2019) 8532.
15. K. Magdić Košiček, K. Kvastek and V. Horvat-Radošević, *J. Solid State Electrochem*., 20 (2016) 3003.
16. R. Aydın and F. Koleli, *Prog. Org. Coat.,* 56 (2006) 76.
17. M. M. El-Deeb, K. Alenezi, H. El Moll, M. El-Masry and Z. Matarneh, *Int. J. Electrochem. Sci*., 12 (2017) 10140.
18. E. Navarro-Flores and S. Omanovic, *J. Mol. Catal. A-Chem*., 242 (2005) 182.
19. A. Damian and S. Omanovic, *J. Power Sources,* 158 (2006) 464.
20. D. A. Dalla Corte, C. Torres, P. dos Santos Correa, E. Schmidt Rieder and C. de Fraga Malfatti, *Int. J. Hydrogen Energy*, 37 (2012) 3025.
21. C. Torres, B. Moreno, E. Chinarro and C. de Fraga Malfatti, *Int. J. Hydrogen Energy*, 42 (2017) 20410.
22. N. Zhang, W. Ma, T. Wu, H. Wang, D. Han and L. Niu, *Electrochim. Acta*, 180 (2015) 155.
23. A. Kellenberger, N. Plesu, M. Tara-Lunga Mihali and N. Vaszilcsin, *Polymer,* 54 (2013) 3166.
24. A. Kellenberger, D. Ambros and N. Plesu, *Int. J. Electrochem. Sci.,* 9 (2014) 6821.
25. M. Žic, *J. Electroanal. Chem*., 635 (2009) 29.
26. Z. Mandić, M. Kraljić Roković and T. Pokupčić, *Electrochim. Acta*, 54 (2009) 2941.
27. A.G. MacDiarmid and A.J. Epstein, *Faraday Discuss. Chem. Soc.*, 88 (1989) 317.
28. E. M. Geniès and M. Lapkowski, *J. Electroanal. Chem.,* 220 (1987) 67.
29. D.E. Stilwell and S.M. Park, *J. Electrochem. Soc*., 135 (1988) 2254.
30. Lj. Arsov, W. Plieth and G. Koßmehl, *J. Solid State Electrochem*., 2 (1998) 355.
31. K. Darowicki and J. Kawula, *Electrochim. Acta*, 49 (2004) 4829.
32. G. Inzelt, *Electrochim. Acta,* 45 (2000) 3865.
33. E. M. Geniès, M. Lapkowski and J.F. Penneau, *J. Electroanal. Chem. Interf. Electrochem.*, 249 (1988) 97.
34. E. Dmitrieva, Y. Harima and L. Dunsch, *J. Phys. Chem. B*, 113 (2009) 16131.
35. C.C. Vaduva, N. Vaszilcsin, A. Kellenberger and M. Medeleanu, *Int. J. Hydrogen Energy*, 36 (2011) 6994.
36. C.C. Vaduva, N. Vaszilcsin and A. Kellenberger, *Int. J. Hydrogen Energy*, 37 (2012) 12089.
37. R. Cretu, A. Kellenberger and N. Vaszilcsin, *Int. J. Hydrogen Energy*, 38 (2013) 11685.
38. R. Cretu, A. Kellenberger, M. Medeleanu and N. Vaszilcsin, *Int. J. Electrochem. Sci*., 9 (2014)

4465.
39. H. Gerischer, Principles of Electrochemistry in The CRC Handbook of Solid State Electrochemistry, P. J. Gellings and H. J. M. Bouwmeester (Editors), CRC Press, Boca Raton, New York, 1997.
40. P. Zhu and Y. Zhao, *Adv. Eng. Mater.*, 19 (2017) 1700392.
41. X. Mo, J. Wang, Z. Wang and S. Wang, *Synth. Met.*, 142 (2004) 217.